Particle Identification I

Jürgen Engelfried

Instituto de Física, Universidad Autónoma de San Luis Potosí, Mexico
email: `jurgen@ifisica.uaslp.mx`

Abstract. This is a write-up of a course given a the "First ICFA Instrumentation School/Workshop at the ICFA Instrumentation Center in Morelia, Mexico", November 18-29, 2002, University of Michoacan, Morelia, Mexico. We will concentrate on Transition Radiation and Ring Imaging Cherenkov detectors, since other particle identification methods are discussed in other courses. We describe the principle design of these detectors and discuss specific examples.

INTRODUCTION

In this 2 hour course we will discuss the identification of charged particles only. Identification of neutral particles is covered by the calorimetry course.

For general knowledge of particle detector, see the common literature, for example [1, 2, 3]. On a more compressed summary, see [4].

In general there are two major applications for particle identification: 1) Identification of beam particles, especially for Fixed Target Experiments and 2) Identification of decay products. In both cases the momentum of the particle is know, either selected naturally by the beam line elements in a small momentum bin, or by a magnetic spectrometer, which is covered in the tracking detector course.

With the momentum of the particle known, particle identification reduces to measure the velocity, which is covered in this class, the total energy (covered in the calorimeter class), or the specific energy loss dE/dx.

As an appetizer, we will first discuss a typical example where particle identification is crucial in physics analysis. Here we will discuss the reconstruction of $\Lambda_c^+ \to pK^-\pi^+$ and the corresponding antiparticle decay. The Λ_c^+ is a baryon consisting of (udc) quarks, with a mass of $2.2849\,\mathrm{GeV}/c^2$ and a lifetime of $\tau = 2.0 \cdot 10^{-13}\,\mathrm{s}$. The decay mode used here has a branching ratio of 5 %, and it should be remembered that the charm production cross section is about 1/1000 of the total cross section. With special relativity, especially the time dilation, we can easily calculate that a Λ_c^+ with a momentum of $200\,\mathrm{GeV}/c$ will have an average flight path of 5.4 mm – easily measurable with the help of silicon microstrip detectors in a Fixed Target experiment. But: The Λ_c^+ will decay before it reaches the first detectors, so we can only measure the decay products.

If we measure type, direction, momentum, and charge of all decay products, and apply momentum and energy conservation to "interesting" decay vertices we can calculate the energy and momentum (the quadrivector) of the hypothetical mother particle. In the rest system of the mother particle this is the rest mass. We will do this for a lot of events, fill a histogram, and hope that a peak will evolve in the distributions of the invariant mass at the correct place.

The direction of the tracks and the decay vertex are measured by silicon microstrip detectors, the momentum and charge by a magnetic spectrometer, and the velocity in a RICH detector via the ring radii (see later in this class). In addition, the beam particle which initiates the charm production is identified by a Beam Transition Radiation Detector. At the end we obtain distributions in invariant mass, one for each beam particle, as shown in fig. 1.

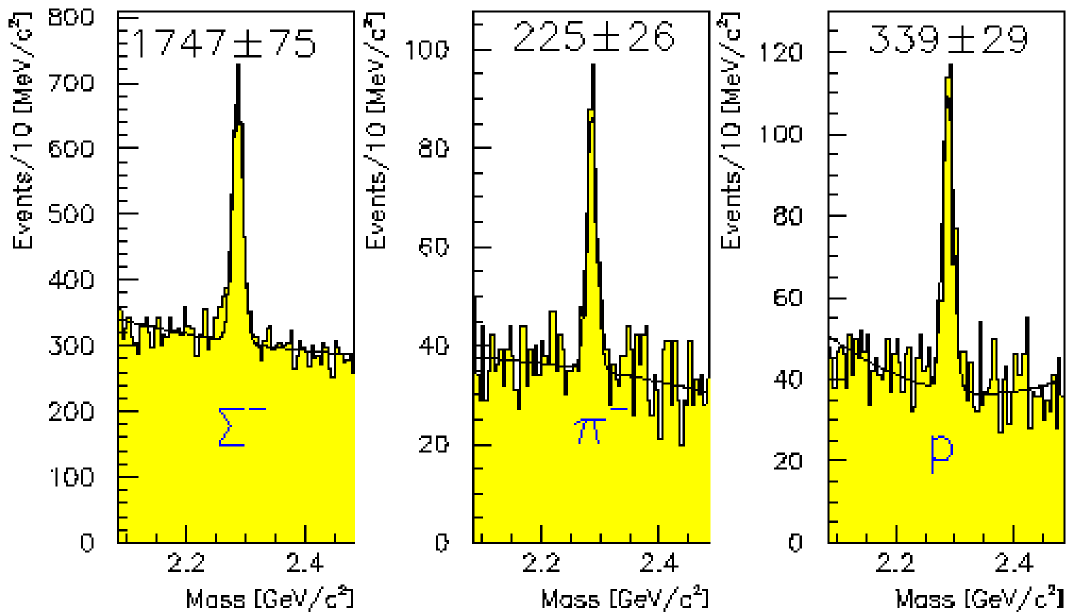

FIGURE 1. Invariant mass distributions for $\Lambda_c^+ \rightarrow pK^-\pi^+ + \text{c.c.}$ with identified beam particle and decay products from SELEX [5]

TIME–OF-FLIGHT (TOF)

This method of particle identification is discussed in the lecture of E. Nappi. The method is in principal very simple: put two scintillation counter at a know distance, and measure the time difference between the signals from the two counters, and you get the velocity. A good time resolution is in the order of 150 ps, and typical distances are 10 m in detectors and 100 m in beam lines. Kaons and pions can be differentiated up to a few GeV with TOF.

In addition to the limited momentum range, TOF also has problems at high rates and/or multiple particles hitting the same scintillator.

RADIATION BY CHARGED PARTICLES

Radiation is emitted by a charge particle if:

1. $|\vec{v}| > c/n$: *Cherenkov Radiation*

2. $\vec{v}/c_{\text{ph}} = \vec{v} \cdot n/c$ changes
   (a) $|\vec{v}|$ changes: *Bremsstrahlung*
   (b) direction of $\vec{v}$ changes: *Synchrotron Radiation*
   (c) n changes: *Transition Radiation*

Here $\vec{v}$ is the velocity of the particle, c the speed of light in vacuum, and n the refractive index of the medium. In this course, we will discuss in detail the cases of Transition Radiation and Cherenkov radiation, since there are velocity dependent effects, which will help us (with known momentum) in the identification problem.

TRANSITION RADIATION DETECTORS (TRD)

Transition radiation is emitted due to the reformation of the particle field if it crosses a boundary between two media with dielectrical constants ε_1 and ε_2. The total energy S of radiation emitted at a single interface is given by

$$S = \frac{\alpha\hbar Z^2}{3}\frac{(\omega_1 - \omega_2)^2}{\omega_1 + \omega_2}\gamma \tag{1}$$

where $\alpha = 1/137$ (the fine structure constant), ω_1 and ω_2 the plasma frequencies, and $\gamma = E/mc^2$ (the relativistic γ). Typical values for the plasma frequencies are: in air $\omega_1 = 0.7\,\text{eV}$, in polypropylene $\omega_2 = 20\,\text{eV}$. The spectral (ω) and angular (ϑ) dependence of the Transition Radiation is given by

$$\frac{d^2}{d\vartheta d\omega} = \frac{2e^2}{\pi c}\left(\frac{\vartheta}{\gamma^{-2} + \vartheta^2 + \omega_1^2/\omega^2} - \frac{\vartheta}{\gamma^{-2} + \vartheta^2 + \omega_2^2/\omega^2}\right)^2 \tag{2}$$

Most of the radiation is emitted in a cone with half angle $1/\gamma$ in the forward direction of the particle.

In fig. 2 we show a measurement of the spectral distribution of Transition Radiation, which can be compared to eq. 2. For large photon energies ($\omega > \gamma\omega_2 \approx 20 - 30\,\text{KeV}$) we observe a large drop of intensity $\propto \gamma^4/\omega^4$, for medium energies ($\gamma\omega_1 < \omega < \gamma\omega_2$) a logarithmic decrease with ω, and for small energies $\omega < \gamma\omega_1 \approx 1\,\text{KeV}$ a almost constant intensity. The vertical scale tells us that the probability to emit a KeV photon in $\approx 10^{-2}$. The get this to unity, we need a lot of interfaces: Usually one uses a stack of radiator foils.

In any case one needs a minimum foil thickness so the particle field can reach a new equilibrium. Since we have now two transitions (into and out off the foil) which are equal ($\omega_1 \to \omega_2$ and $\omega_2 \to \omega_1$) we see interference effects as maxima and minima in fig. 2. If we space the foils in the stack in equal distances, we can expect in addition interference between the amplitudes of different foils. As a disadvantage we observe a re-absorption of the radiation due to the finite thickness of the foils, which is $\propto Z^5$, so usually low Z materials like Mylar, CH_2, carbon fibers, lithium are used as foils, with a thickness of 30μm and foil distances of 300μm.

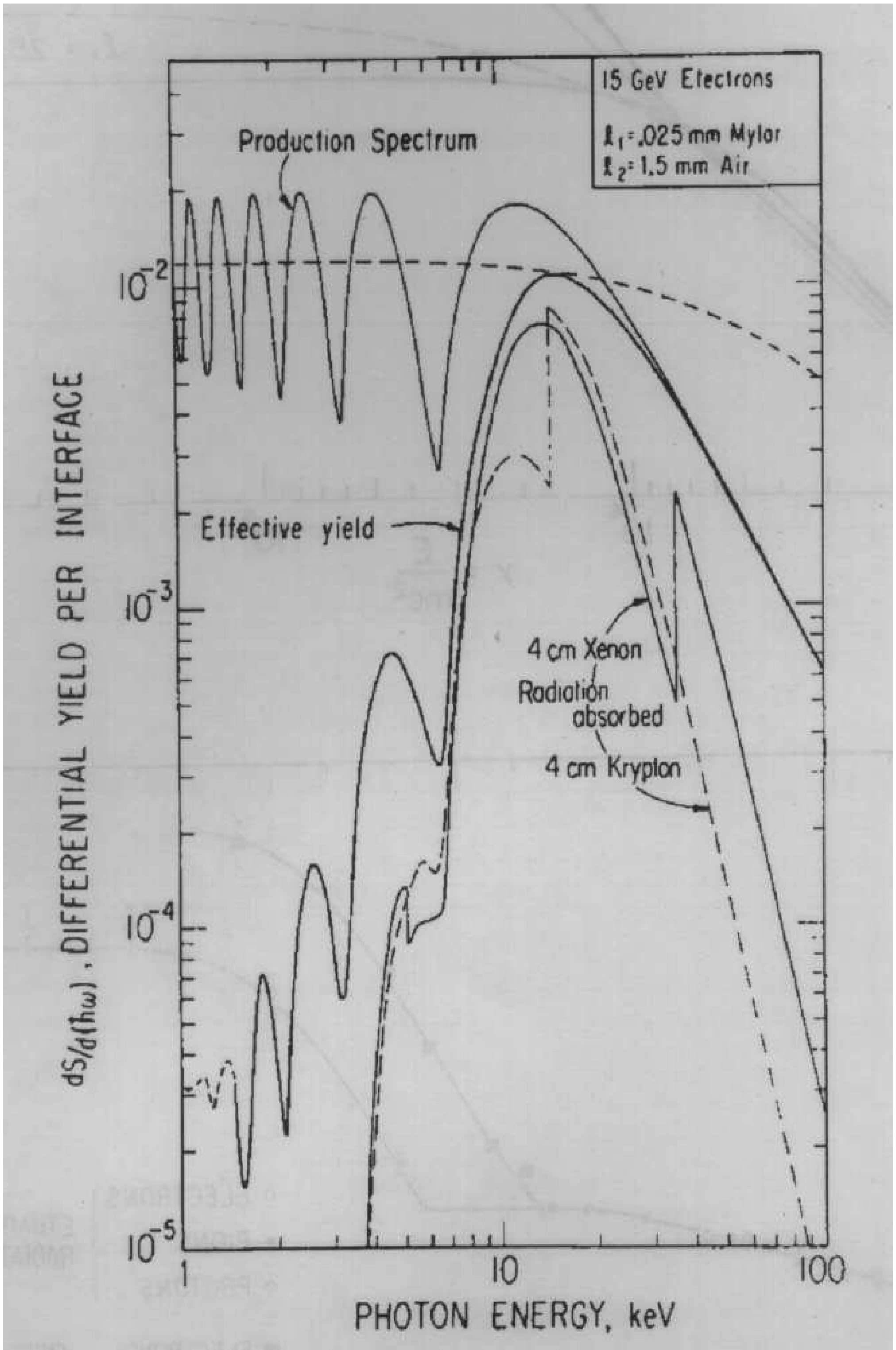

FIGURE 2. Spectral Distribution of Transition Radiation. For details see text and [12]

DETECTION OF TRANSITION RADIATION

As mentioned before, the X-ray photons from Transition Radiation are emitted under a small angle to the particle track, so whatever detector we will place to detect the X-rays will be traversed by the particle itself too, leaving an additional dE/dx energy loss in the detector. Typical dE/dx in gas detectors is some KeV/cm and is Landau distributed, so that signals from dE/dx and the X-rays are very similar. A detector consists typically of a "thin" MWPC, with Xenon or Krypton as gas, and several (10-30) radiator / chamber units so one can beat the Landau distribution. In fig. 3 we show two

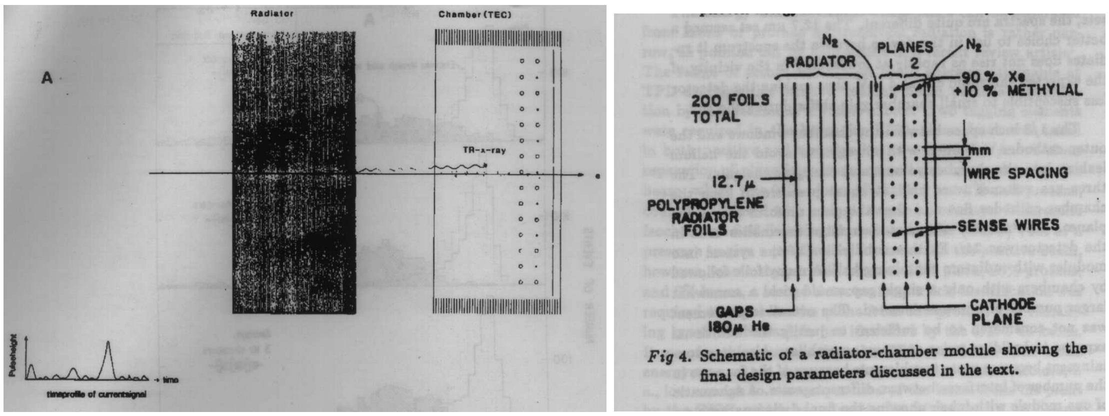

FIGURE 3. Examples for one unit of a Transition Radiation Detector (from [12] (left) and [10, 11] (right).

examples of Transition Radiation detectors [12] and [10, 11].

To separate the signals, and to discriminate between the (Landau-distributed) dE/dx and the absorbed X-ray signal, two different analysis methods, which also translate to specifications on the readout electronics, are used: Charge Integration and Cluster Counting.

The Charge Integration method measures the total charge of the ionization in every unit, and counts how many chambers saw a total charge larger than some given threshold.

The Cluster Counting method employs the different spatial ionization distribution of the two source (point for X-ray, line for dE/dx) to separate them.

In figure 4 we show an example of a TRD detector which identifies the beam particles in the SELEX [30] experiment. It consists of 10 units, each of them with three wire planes, and is operated in the Charge Integration mode. The electronics used is seen on the bottom.

The obtained signals (either clusters or charge) are compared with a likelihood method to different particle hypothesis, with known momentum. The most probable hypothesis is selected for the identification. In fig. 5(left) we show as example the number of planes in the SELEX BTRD which are above threshold. Clearly two peaks are seen, associated with Σ^-, which have a small number of planes fired, only due to the Landau fluctuations, and to the π^-, which emits significant transition radiation and fired more planes. On the right plot we compare the efficiency to identify Σ^- and π^- for a simple counting method, and a sophisticated likelihood method.

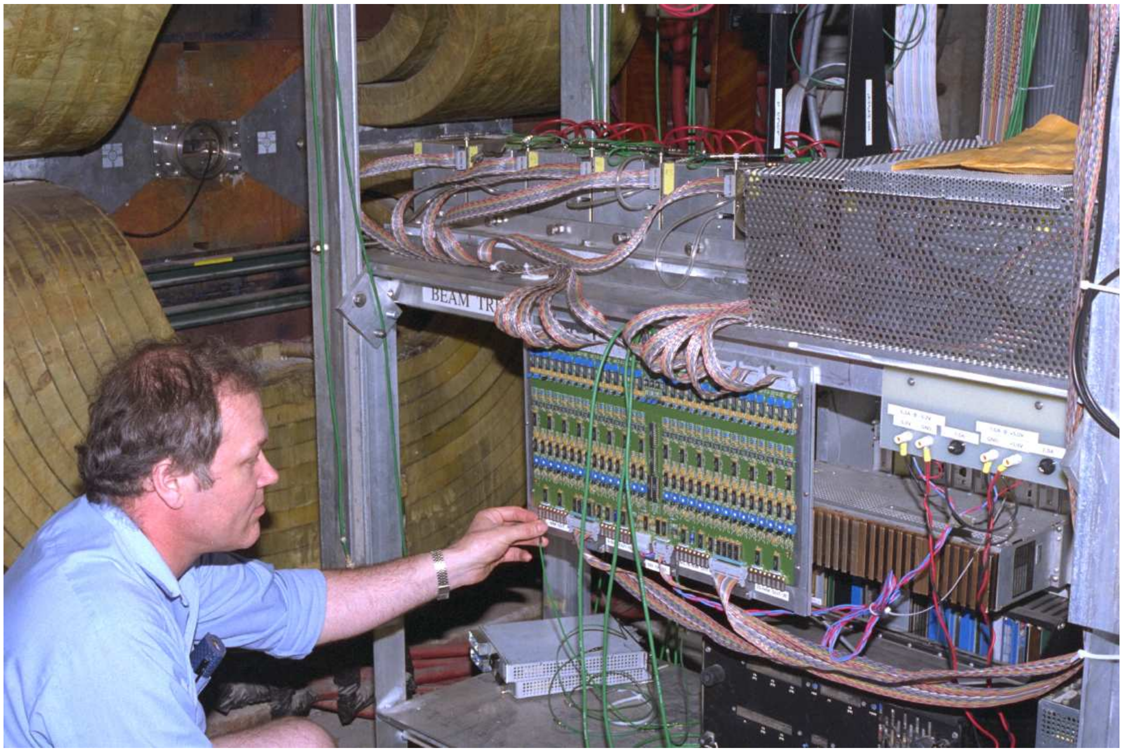

FIGURE 4. The SELEX Beam Transition Radiation Detector.

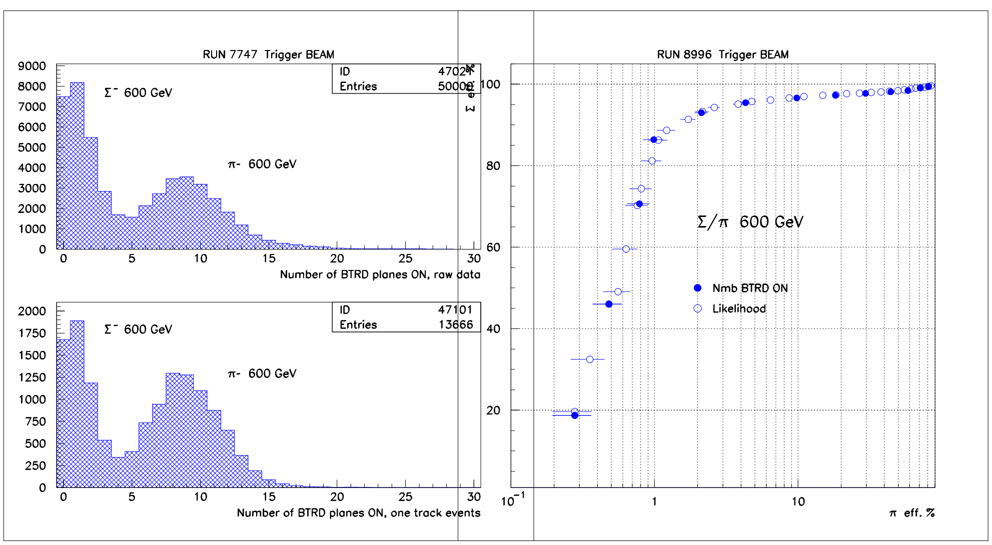

FIGURE 5. Left: Distribution of number of SELEX BTRD modules with a charge larger than a threshold, for two different cuts. Right: Efficiency for identifying Σ^- and π^- beam particles with $600\,\mathrm{GeV}/c$ with the SELEX BTRD for a simple counting and a sophisticated likelihood algorithm [7]

THE ATLAS TRANSITION RADIATION TRACKER (TRT)

The most extreme and sophisticated usage of TRD technology is planned for the ATLAS experiment at the LHC. They will use more than 370,000 straw tubes as transition radiation detector and in addition use the information for tracking [8]. This is an enormous enterprise. Some data are given in fig. 6.

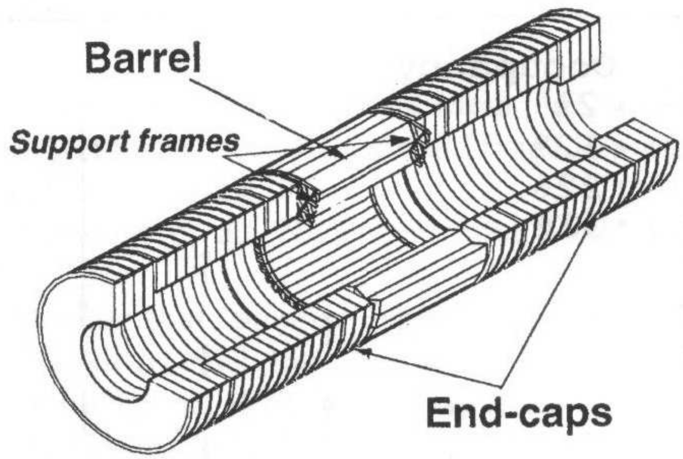

Length:	Total	6802 cm	N straws:	Total	372032
	Barrel	148 cm		Barrel	52544
	End-cap	257 cm		End-cap	319488
Outer diameter		206 cm	N electronics channels		424576
Inner diameter		96-128 cm	Weight		~ 1500 kg

Fig. 11. ATLAS Transition Radiation Tracker (TRT) conceptual design [2].

FIGURE 6. Figure taken from [8].

CHERENKOV RADIATION

Even though the basic idea of determining the velocity of charged particles via measuring the Cherenkov angle was proposed in 1960 [13], and in 1977 a first prototype was successfully operated [14], it was only during the last decade that Ring Imaging Cherenkov (RICH) Detectors were successfully used in experiments. A very useful collection of review articles and detailed descriptions can be found in the proceedings of four international workshops on this type of detectors, which were held in 1993 (Bari, Italy) [15], 1995 (Uppsala, Sweden) [16], 1998 (Ein Gedi, Israel) [17], and 2002 (Pylos, Greece) [18], respectively.

Charged particles with a velocity $|\vec{v}|$ larger than the speed of light in a medium with refractive index n will emit Cherenkov radiation under an angle θ, given by [19]

$$\cos\theta = \frac{1}{\beta n} \tag{3}$$

with $\beta = v/c$, c being the speed of light in vacuum. The number of photons N emitted per energy interval dE and path length dl is given by [20]

$$\frac{d^2N}{dEdl} = \frac{\alpha}{\hbar c}\left(1 - \frac{1}{(\beta n)^2}\right) = \frac{\alpha}{\hbar c}\sin^2\theta \tag{4}$$

or, expressed for a wavelength interval $d\lambda$,

$$\frac{d^2N}{d\lambda dl} = \frac{2\pi\alpha}{\lambda^2}\sin^2\theta \tag{5}$$

A first (obvious) application are Threshold Cherenkov Counters. For a fixed momentum, and only two particle types to separate, one chooses a medium with appropriate index of refraction, with a threshold between the velocity of the two particles. If one detects any light, the lighter particle passed. For more than 2 particle types and/or a wider momentum range to cover, several counters with different thresholds have to employed.

By measuring the Cherenkov angle θ one can in principle determine the velocity of the particle, which will, together with the momentum p obtained via a magnetic spectrometer, lead to the determination of the mass and therefore to the identification of the particle[1].

Neglecting multiple scattering and energy loss in the medium, all the Cherenkov light (in one plane) is parallel, and can therefore be focused (for small θ) with a spherical mirror (radius R) onto a point, as shown in fig. 7. Since the emission is symmetrical in the azimuthal angle around the particle trajectory, this leads to a ring of radius r in the focus, which is itself a sphere with radius $R/2$. The radius r is given by

$$r = \frac{R}{2}\tan\theta \tag{6}$$

---

[1] For this reason Cherenkov detectors are usually described under the chapter "particle identification" in particle detectors books.

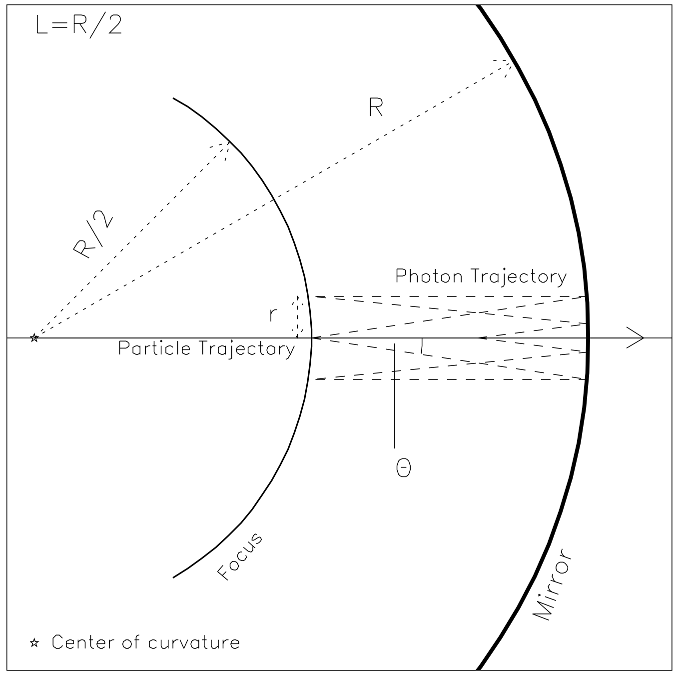

FIGURE 7. Schematic of a RICH detector

$$r \approx \frac{R}{2}\sqrt{2 - \frac{2}{n}\sqrt{1 + \frac{m^2c^2}{p^2}}} \tag{7}$$

The dependence of the ring radius on the momentum for different particles is shown in fig. 8 All these features can obviously been measured, as is shown in fig. 9, were more than 53 million tracks, with their momentum and ring radius measured, were used [37]. A similar plot was obtained for positive tracks, 16 particles and antiparticles could be identified.

A SHORT HISTORY OF RICHES

After the first successful laboratory tests in the 1970's [14], at the beginning of the 1980's the first generation of Ring Imaging Cherenkov Detectors were built, with mixed results. Examples are The CERN Omega RICH, used by WA69 and WA82 [22], the UA2 RICH at CERN, and the E653 RICH at Fermilab.

A second generation RICH detectors were developed and employed at the end of the 80's and beginning of the 90's, with the experiences (positive and negative) from the first generation incorporated. Examples are an upgraded Omega RICH, used by WA89 and WA94 [22], Delphi, CERES (all at CERN), and the SLD–GRID at SLAC. All these

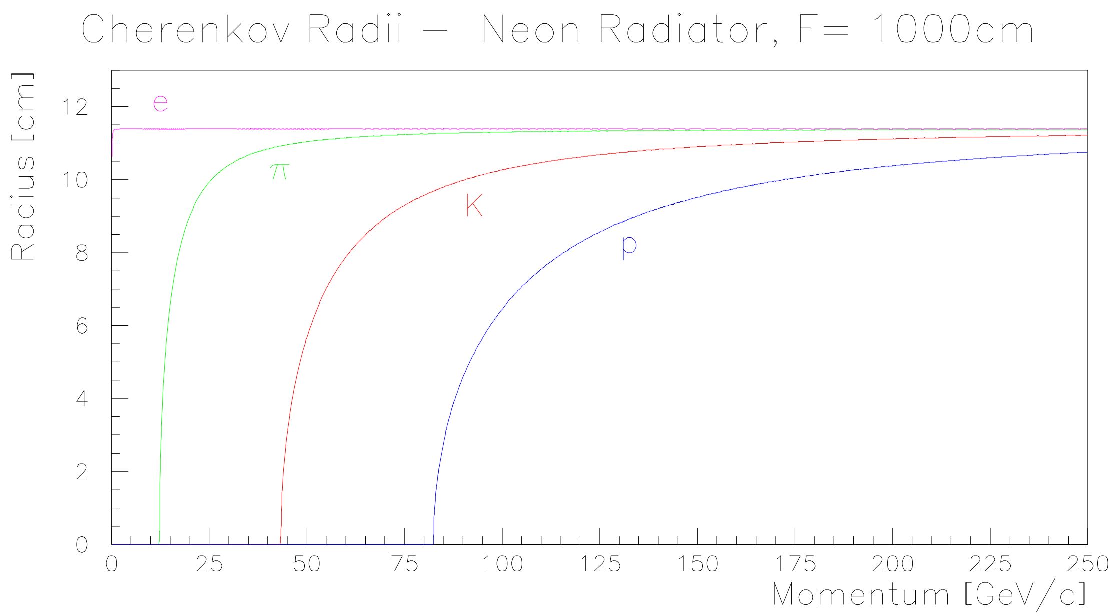

FIGURE 8. Ring radii for different particles as a function of momentum, in the case of the SELEX RICH detector ($R = 1982\,$cm, radiator Neon at atmospheric pressure).

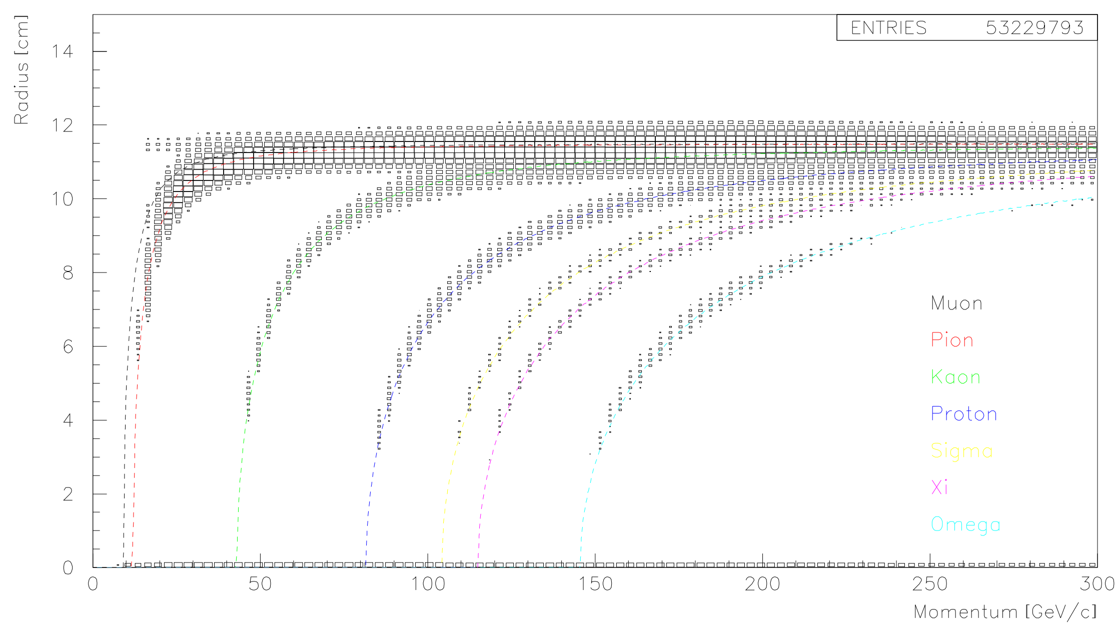

FIGURE 9. Radius of rings versus momentum measured by the SELEX RICH. 53 million negative tracks were used. We can clearly identify 8 different particle types.

detectors had significant startup problems to overcome, but eventually they all worked very well and contributed to the physics analysis of the experiments.

The third generation, build and used mid-end 90's, finally worked without too many problems from the beginning and all of them played an important role in the physics analysis. Examples are the SELEX RICH at Fermilab, and Hermes and Hera-B at DESY.

Since the mid-90's, the RICHes are an established detector type, and is currently employed in recent experiments: BaBar–DIRC (SLAC), PHENIX (Brookhaven-RHIC), CLEO–III (Cornell), COMPASS (CERN).

There is a long list of future experiments, who plan to or are already building RICHes: ALICE, LHC–B (CERN), BTeV, CKM (Fermilab), and many more. Also in other fields like nuclear physics (GSI) and in astroparticle physics experiments technology developed for RICHes is used.

GENERAL DETAILS FOR RICHES

Since the number of photons is $\propto \lambda^{-2}$ (eq. 5), most of the light is emitted in the VUV range. To fulfill equation 3, the refractive index has to be $n > 1$, so there will be no Cherenkov radiation in the x-ray region. Also it is very important to remember that n is a function of the wavelength ($n = n(\lambda)$, chromatic dispersion) and most materials have a absorption line in the VUV region, where $n \to \infty$, as shown in fig. 10, using Neon as example. Since usually the wavelength of the emitted photon is not measured, this

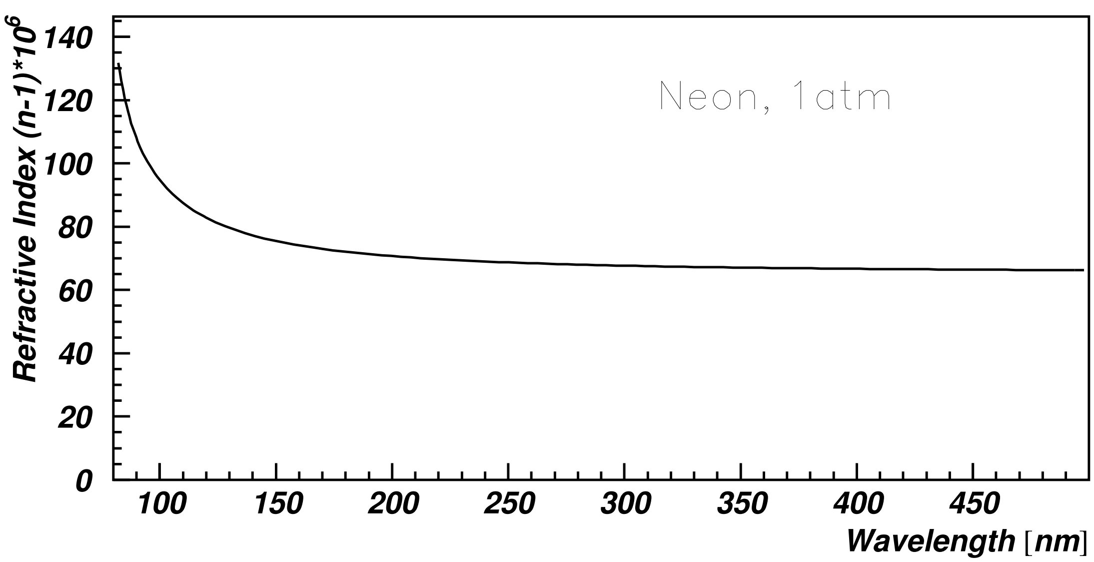

FIGURE 10. Refractive index $n-1$ for Neon as a function of wavelength at STP [21].

leads to a smearing of the measured ring radius, and one has to match carefully the wavelength ranges which one wishes to use: Lower wavelengths gives more photons, but larger chromatic dispersion.

A very useful formula is obtained by integrating eq. 5 over λ (or E), taking into account all efficiencies etc., obtaining a formula for the number of detected photons

N_{ph} [14]:

$$N_{ph} = N_0 L \sin^2 \theta \tag{8}$$

where N_0 is an overall performance measure (quality factor) of the detector, containing all the details (sensitive wavelength range, efficiencies), and L is the path length of the particle within the radiator. A " very good" RICH detector has $N_0 = 100\,\mathrm{cm}^{-1}$, which gives typically around 10 to 15 detected photons (N_{ph}) per $\beta = 1$ ring.

The usual construction of a RICH detector is to use a radiator length of $L = R/2$, e.g. equal to the focal length; but any other configuration, like folding the light path with additional (flat) mirrors, is possible.

All the presented arguments and the drawing in fig. 7 only work for small θ, which is always fulfilled in gases, since n only differs little from 1. Also important is the fact, that, should the particles not pass through the common center of curvature of mirror(s) and focal spheres, the ring gets deformed to an ellipse or, in more extreme cases, to a hyperbola. If the photon detector is able to resolve this, and the resolution is needed for the measurement, these deviations from a perfect circle have to be taken into account in determining the velocity β. In general this effect can be neglected, and all parallel particles (with the same β) will give the same ring in the focal surface, due to the fact that all emitted Cherenkov light is parallel. The position of the ring center is determined by the angle of the tracks, not by their position.

In the following, we will describe three RICH detectors used in experiments, and a new application for RICH detectors for a new experiment. The selection is clearly biased by the author, but even so, we feel that they are good examples for the use of this kind of detectors.

THE CERN OMEGA-RICH

In the middle of the 1980's, first attempts were made to apply the prototype results obtained by Séguinot and Ypsilantis [14] to experiments in a larger scale. One of these attempts was performed at the CERN Omega facility in the West Hall. Experiments WA69 and WA82 tried to use this detector for there analysis, but only succeeded partly. An overview about this history can be found in [22]. When in 1987 a new experiment, later named WA89, was proposed [23, 24], an important part was a necessary upgrade of this detector for the use by this new experiment. Two main parts where changed: New photon detectors using TMAE as photo sensitive component, and new mirrors to perform the focusing. Details about the detector can be found in [22, 25, 26, 27, 28].

As seen in the overall layout of the detector (fig. 11), a RICH detector is basically a simple device: a big box, some mirrors at the end, and photon-sensitive detectors at the entrance. The real challenge is to combine all the parameters together to obtain a perfect match for the overall system.

The size of the radiator box and the photon detector is given by the angular distribution of tracks which have to be identified at the location of the detector. Since usually this detector is placed behind a magnetic spectrometer, and the momentum spectrum of the interesting tracks depends on the physics goals of the experiment, the surfaces to cover have to be determined for every setup and experiment, usually with Monte Carlo

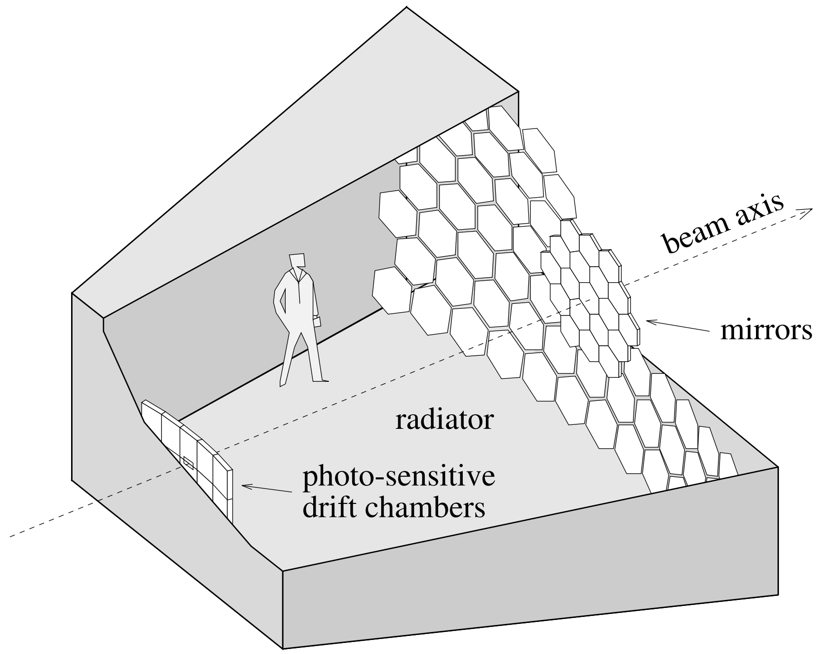

FIGURE 11. Overall view of the CERN Omega RICH detector, used in experiment WA89. The radiator gas is pure Nitrogen, so usually there is no person within the radiator box.

simulations during the design phase of the experiment [25]. In the case of WA89, the mirror surface needed was about $1\,\mathrm{m} \times 1.5\,\mathrm{m}$, much smaller than the $4\,\mathrm{m} \times 6\,\mathrm{m}$ covered by the original Omega-RICH. It was therefore decided to replace only the central mirrors with smaller (as seen in fig. 11), higher surface quality mirrors to obtain better resolution.

The detector surface was calculated to be $1.6\,\mathrm{m} \times 0.8\,\mathrm{m}$, with a spatial resolution of a few millimeters for every detected photon. The pixel size could therefore not be much bigger than also a few millimeters, leading to about 100000 pixels in the detector plane. The solution was to build drift chamber (TPC) modules, shown in fig. 12, covering an area of $35\,\mathrm{cm} \times 80\,\mathrm{cm}$, and approximating the focal sphere with a polygon of 5 modules. After passing a 3 mm thick quartz window (to reduce absorption), the photons hit TMAE (see fig. 13) molecules, converting via photo-effect into an single electron. TMAE is present with a concentration of about $0.1\,\%$ with the driftgas, which is otherwise pure ethan. The use of a quartz window together with TMAE as photo-sensitive gas leads that the detector is only sensitive in a small wavelength range between $165\,\mathrm{nm} < \lambda < 230\,\mathrm{nm}$, as demonstrated in fig. 14. TMAE has a very low vapor pressure, so that at ambient temperatures the molecule is saturated within a gas. To obtain a short enough conversion length of around 1 cm (otherwise the conversion would occur to far away from the focal plane and lead to an addition contribution to the resolution), the drift gas (Ethan) is led through a bubbler, containing TMAE liquid at 30° C. This means that everything after the bubbler, e.g. the whole detector including radiator box, had to be heated to 40° C to avoid condensation. Other unpleasant properties of TMAE include a high reactivity with Oxygen, producing highly electro-negative oxides, which will attach an electron easily, changing the drift velocity by a factor of several thousand, leading to a loss of electrons.

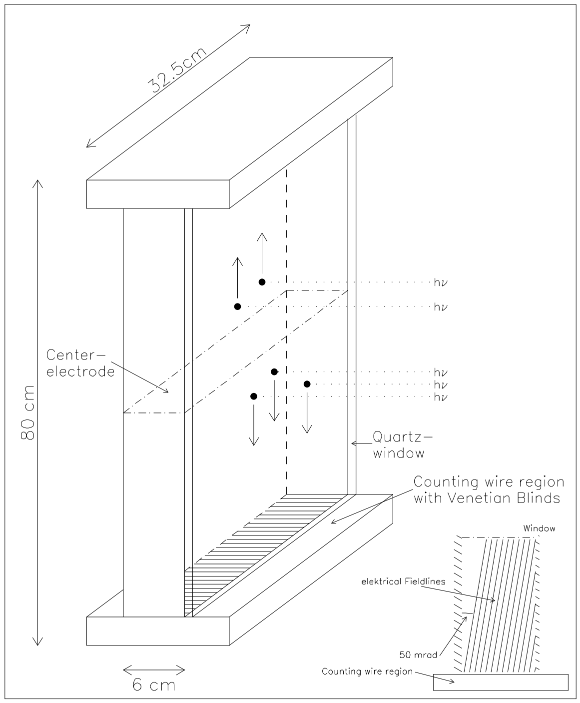

FIGURE 12. Schematic of the Omega-RICH photon detector module. $h\nu$ denotes Cherenkov photons. At the central electrode a voltage of $-40\,\mathrm{kV}$ was applied. The inset shows a side view, demonstrating the electrical field lines (figure taken from [25]).

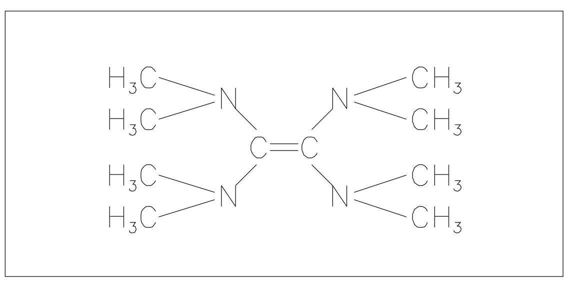

FIGURE 13. Structural formula for Tetrakis(dimethylamino)-ethylen (TMAE). This derivate of Ammonium is the molecule with the lowest ionization energy (5.3 eV).

Since the signal is a single electron (photo-effect!) this is catastrophic. The counting gas had an Oxygen contents of $< 1\,\mathrm{ppm}$.

Mostly due to the presence of TMAE, the operation of this detector was not trivial. All parameters were monitored electronically, and hardware limits on some critical parameters (like temperature, Oxygen content of Ethan) lead to a automatic shutdown of the detector, waiting for an expert to arrive in the experimental hall.

Once the electron was released, it was drifting under the influence of an electric field of $1\,\mathrm{kV/cm}$ (drift velocity $5.4\,\mathrm{cm}/\mu\mathrm{m}$) upwards or downwards over maximal $40\,\mathrm{cm}$

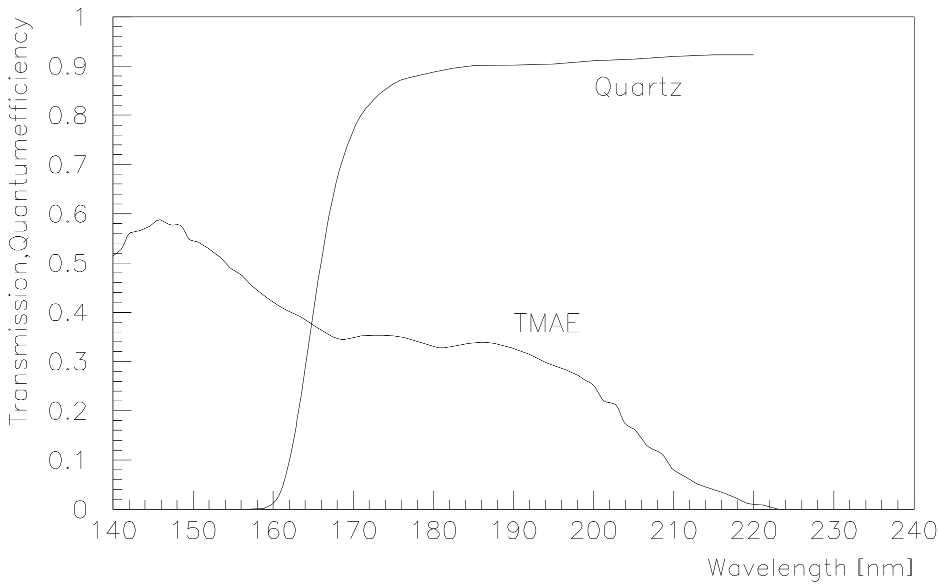

FIGURE 14. Transmission of a quartz window actually used in the Omega-RICH, together with the quantum efficiency (probability of releasing an electron via photo-effect) of TMAE [29], both as a function of wavelength.

toward 6 cm long counting wires (gold-coated tungsten, 15 μm diameter), spaced by 2.54 mm. The two-dimensional spatial information about the conversion point of the photon is obtained with the position of the wire and the drift time of the electron. In total, 1280 wires were used in the detector. An additional complication was that the charged particles itself where passing through the chambers, leaving a dE/dx signal of several hundred electrons, which is to be compared to the single electron which is our signal. This leads to increased requirements for the wire chambers (sensitive, e.g. sufficient multiplication, to single electrons, but no sparking with several hundred electrons) and to the preamplifier electronic (not too much dead time after a big pulse).

The overall resolution allowed the separation of pions and kaons up to a momentum of about 100 GeV/c, which was exactly the design goal. This lead to a good number of physics results (about 15 papers), which would not have been possible to obtain without the RICH detector.

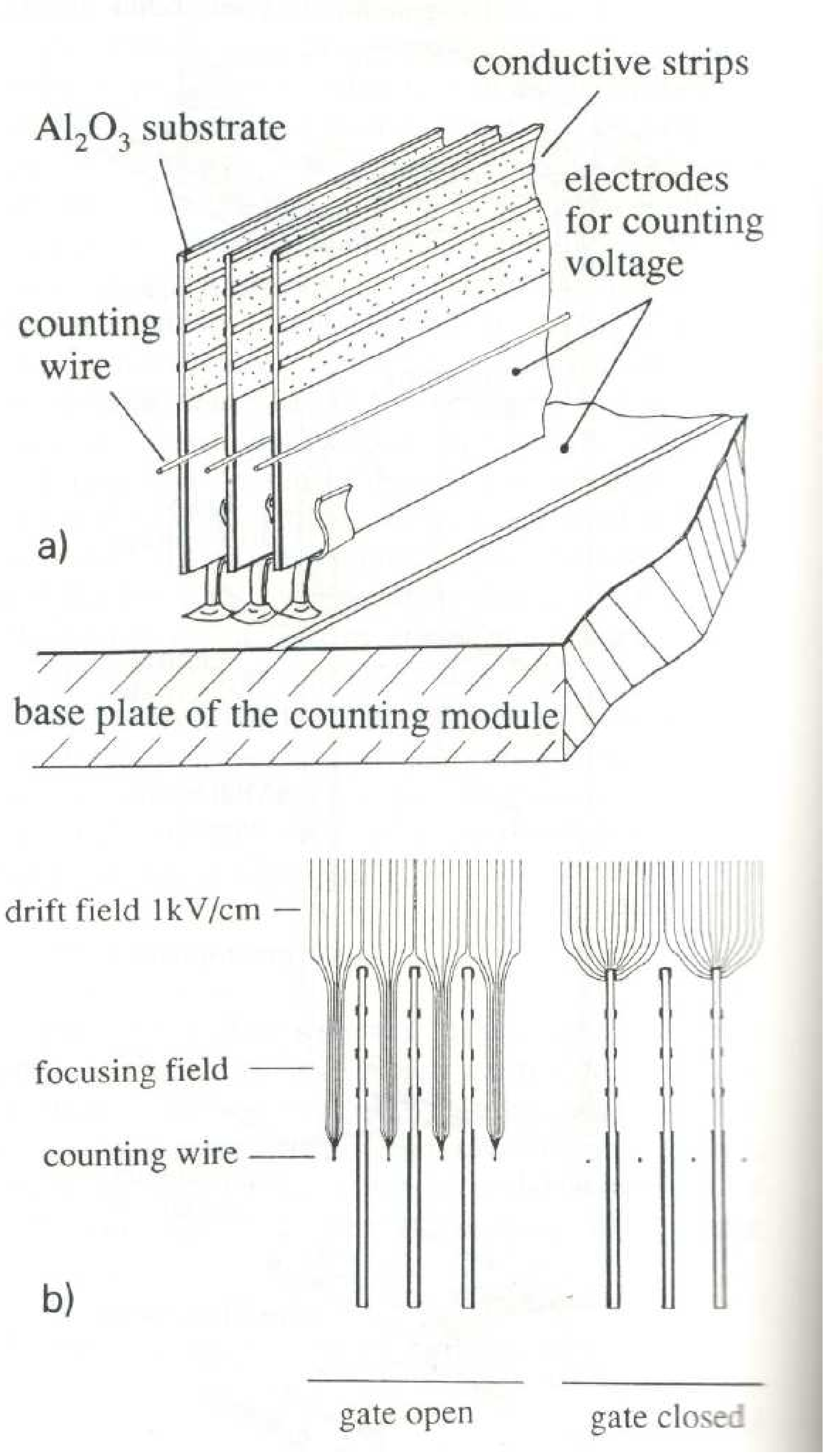

FIGURE 15. Details of the wire arrangement in the WA89 RICH. The uppermost electrodes of the Venetian blinds are pulsed by $\pm 200\,\mathrm{V}$ in case an interesting trigger is received [26].

THE SELEX PHOTOTUBE RICH DETECTOR

At Fermilab an new hyperon beam experiment, called SELEX, was proposed in 1987 [30]. The key elements to perform a successful charmed-baryon experiments are 1) a high resolution silicon vertex detector and 2) a extremely good particle identification system based on RICH. During the following years, a prototype for the SELEX RICH was constructed and tested successfully [31], based in some part on experience gained by our Russian collaborators [32, 33]. The real detector was constructed in 1993-1996, ready for the SELEX data taking period from July 1996 to September 1997. First results for the final detector were reported in [35], and further publications contain all details and performance descriptions of this detector [34, 36, 37].

A layout of the vessel is shown in fig. 16. The radiator gas is Neon at atmospheric

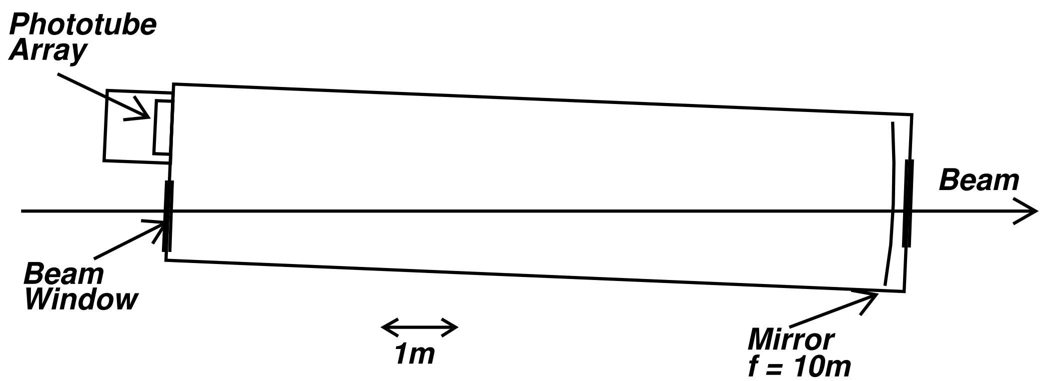

FIGURE 16. Layout of the SELEX RICH detector. The vessel has an overall length of a little over $L = 10\,\mathrm{m}$, the mirrors have a radius of $R = 1982\,\mathrm{m}$. The whole vessel is tilted by $2.4°$ to avoid that the particle trajectories go through the photomultipliers [34].

pressure and room temperature (see fig. 10), filled into the vessel with a nice gas-system [38]: First the vessel is flushed for about 1 day with CO_2 (a cheap gas). After this the gas (mostly CO_2 and little air) is pumped in a closed system over a cold trap running at liquid Nitrogen temperature, freezing out CO_2 and the remaining water vapor. At the same time Neon gets filled into the vessel to keep the pressure constant. This part of the procedure takes about 1/2 day, and the vessel contains afterward only Neon and about 100 ppm of Oxygen which is removed by pumping the gas over a filter of activated charcoal for a few hours, ending with an Oxygen contents of $< 10\,\mathrm{ppm}$ in the radiator. After this all valves were closed and the vessels sits there for the whole data taking of more than 1 year at a slight ($\approx 1\,\mathrm{psi}$) overpressure.

The mirror array at the end of the vessel is made of 11 mm low expansion glass, polished to an average radius of $R = (1982 \pm 5)\,\mathrm{cm}$, coated with Aluminum and a thin over-coating of MgF_2, which gives $> 85\,\%$ reflectivity at 155 nm. The quality of the mirrors was measured with the Ronchi technique [39] to assure a sufficient surface quality of the mirrors. The total mirror array covers $2\,\mathrm{m} \times 1\,\mathrm{m}$ and consists of 16 hexagonally shaped segments. The mirrors are fixed with a 3-point mount consisting of a double-differential screw and a ball bearing to a low mass honeycomb panel. The mirrors are mounted on one sphere, and were aligned by sweeping a laser beam coming from the center of curvature over the mirrors.

The photo detector is a hexagonally closed packed 89×32 array of 2848 half-inch photomultipliers. A side view is shown in fig. 17. In a 3 in. thick aluminum plate holes

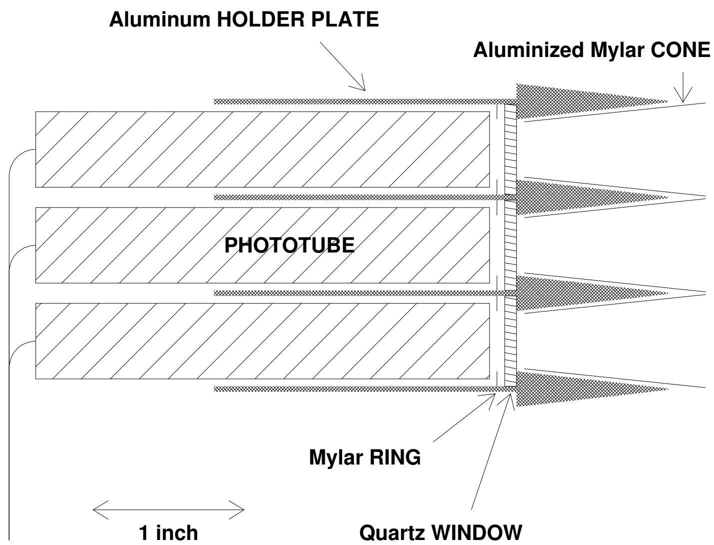

FIGURE 17. Partial cross section through the Phototube Holder Plate. For a more detailed description see text and [34].

are drilled from both sides, a 2 in. deep straight hole holds the photomultiplier, and a conical hole on the radiator side holds aluminized Mylar Winston cones, which form on the radiator side hexagons, leading to a total coverage of the surface. The 2848 holes are individually sealed with small quartz windows. For the central region of the array, a mixture of Hamamatsu R760 and FEU60 tubes were used, in the outside rows only FEU60 tubes are present. The nearly 9000 cables (signal, hv, ground) are routed to the bottom (hv) or top, where the signal cables are connected to preamp-discriminator-ecl-driver hybrid chips and finally readout via standard latch modules[2].

A single event display of the detector is shown in fig. 18, demonstrating the clear multitrack capability and the low noise of this detector. To analyze an event, the ring center is predicted via the known track parameters, and a likelihood analysis [40] for different hypothesis (the momentum is known!) is performed to identify the particle. The final performance for this detector is shown in fig. 19. The detector is nearly 100 % efficient, even below the proton threshold the efficiency is above 90 %. In the SELEX offline analysis, the RICH is one of the first cuts applied to extract physics results.

Up to date, SELEX published 9 papers with physics results from charm and hyperon physics, three of them in PRL.

[2] Since the phototubes are detecting single photons, no ADCs are necessary.

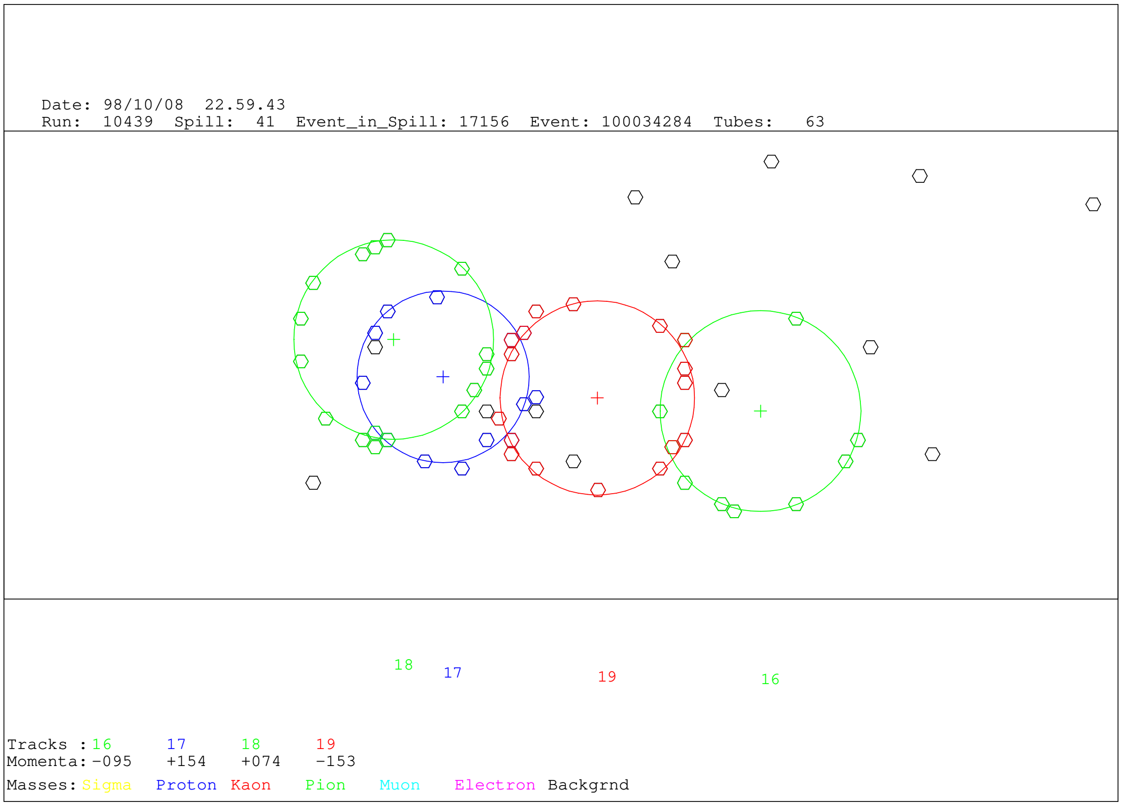

FIGURE 18. Single event display. The small hexagons represent a hit phototube, the circle shows the ring for the most probable hypothesis, and the numbers denote the track numbers, with there momenta shown at the bottom.

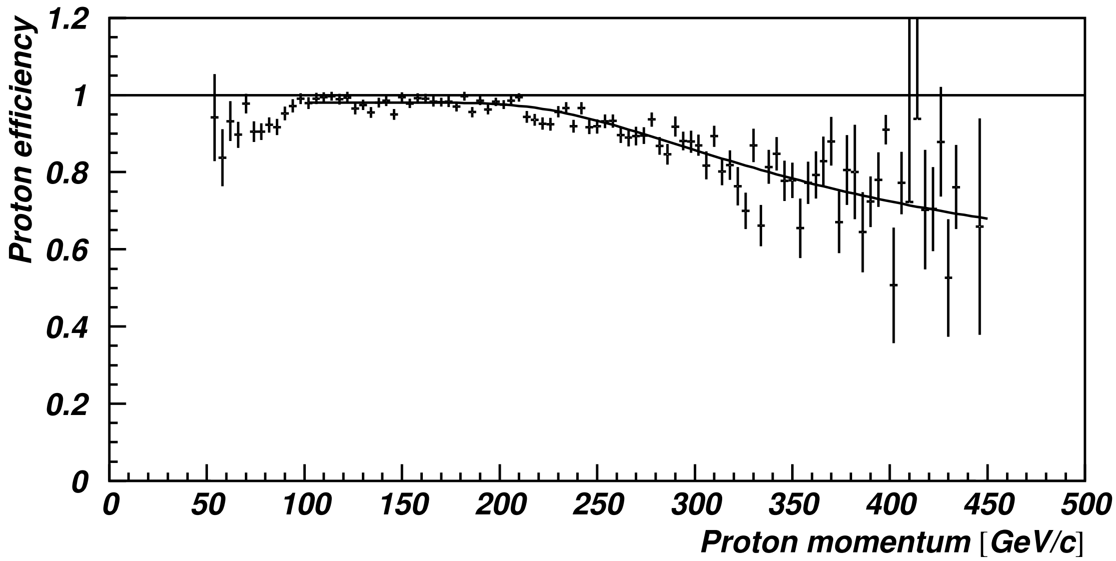

FIGURE 19. Efficiency for identifying a proton as function of its momentum. The likelihood of the track to be a proton has to be at least as big as to be a pion [34].

DIRC AT BABAR

BaBar is an experiment at SLAC, one of the so-called B-Factories, which are measuring in great detail CP-violation parameters in B-Mesons. They employ a RICH detector which they call DIRC (Detection of Internally Reflected Cherenkov light), shown in fig 20. The radiator in this case are quartz bars, which, by internal reflection, transport

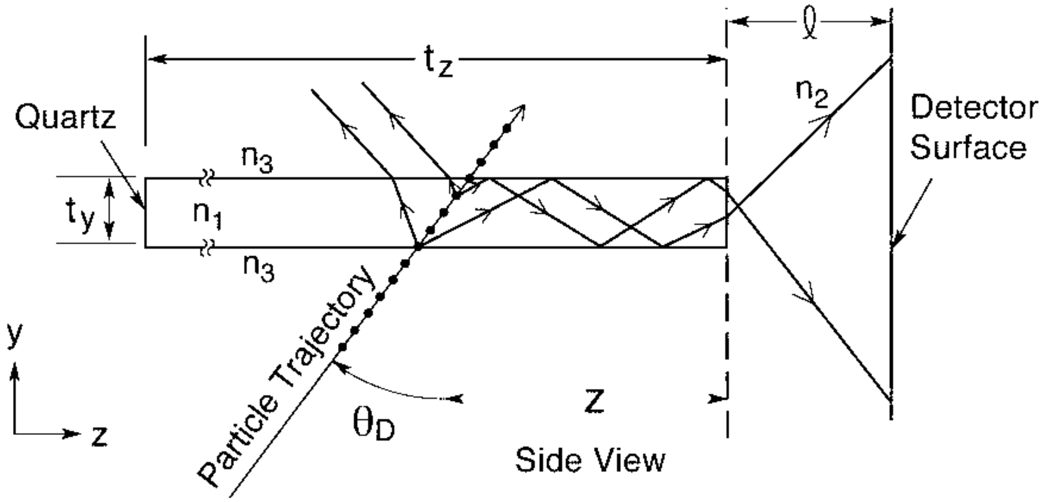

FIGURE 20. Principle design of the DIRC detector at BaBar [41].

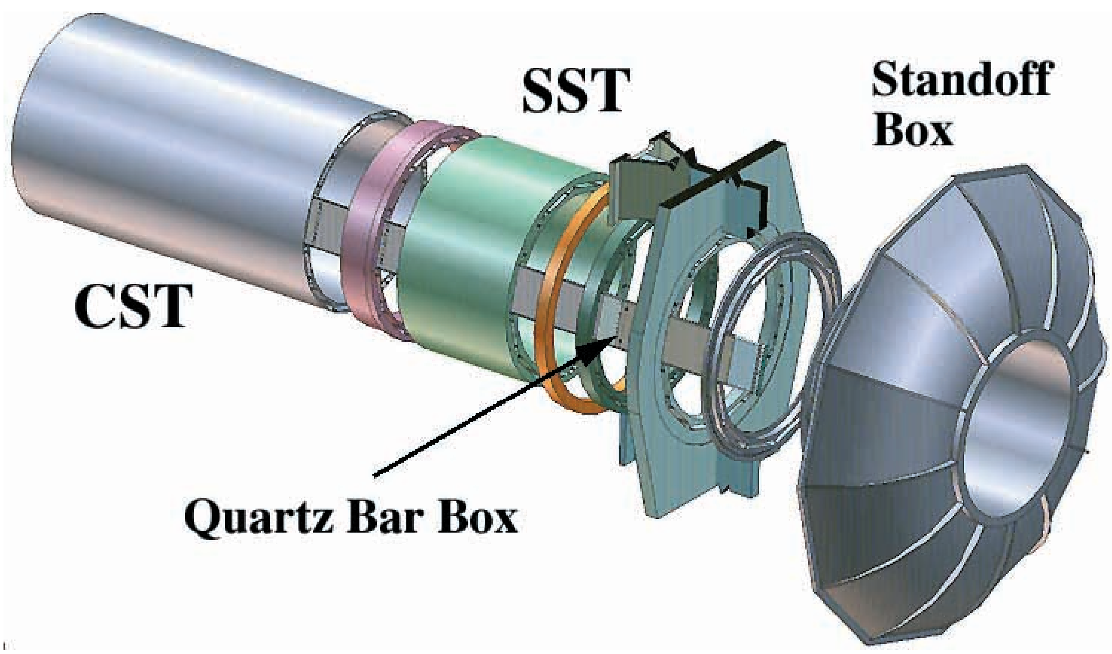

FIGURE 21. Drawing indicating the position of the DIRC within the BaBar Detector.

the Cherenkov light to one side (the other side is mirrored). A standoff box, filled with water, expands the light and couples it to about 10,000 photomultiplier tubes (fig. 21).

Due to the multiple internal reflections, the primary images are not rings, but a more complicated pattern. Nevertheless, by considering in addition the arrival time of the photons at the PMTs, the Cherenkov angle can be reconstructed.

The performance for the DIRC is shown in fig. 22. A clear suppression below the D^0 peak is shown, with a high kaon efficiency and a low miss-identification probability.

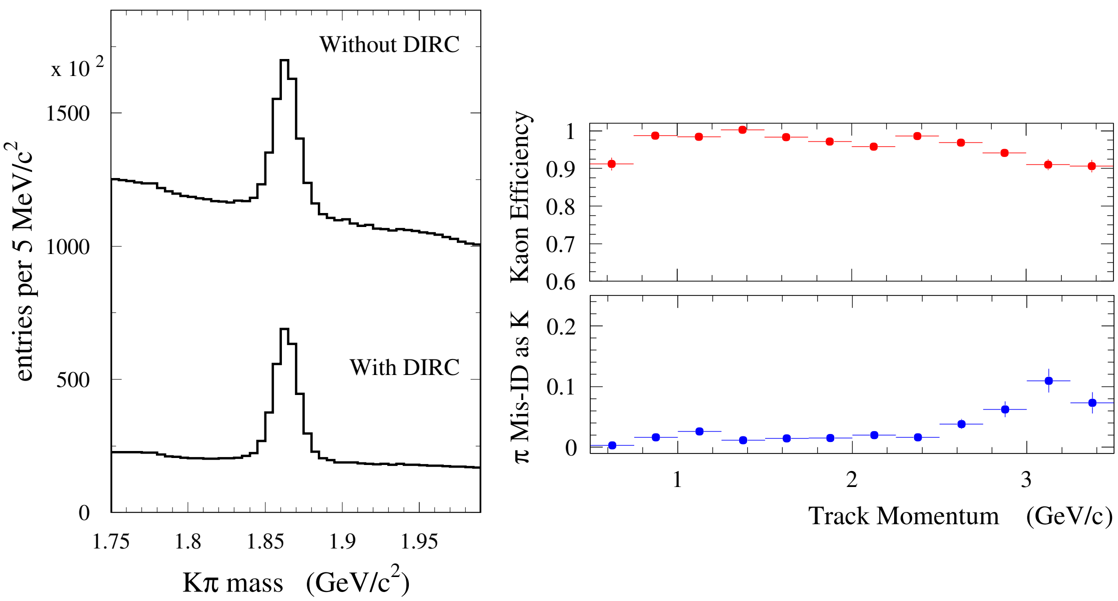

FIGURE 22. Obtained Performance of the BaBar DIRC. Left: $D^0 \to K\pi$ with and without DIRC. Right: Efficiency and miss-identification propability.

More information can be found in [42].

FUTURE OF RICHES WITH A MEXICAN TOUCH: CKM

In 2001, a new experiment called CKM [43] received Stage I approval at Fermilab. The goal of the experiment is to measure the branching ratio for $K^+ \to \pi^+\nu\bar{\nu}$ to an accuracy of 10% (SM prediction is 10^{-10}) to measure the CKM matrix element V_{td}. To withstand the high expected physics background, the experiment will use, in addition to a conventional magnetic spectrometer, a velocity spectrometer consisting of two phototube RICH detectors, one to measure the incoming K^+, the second the outgoing π^+ [44]. The experiment is expected to take data in the second half of this decade.

The expected ring radii for K^+ and π^+ from the beam, measured in the KRICH, are shown in fig. 23. As seen in the figure, the radii are very well separated, so the usual

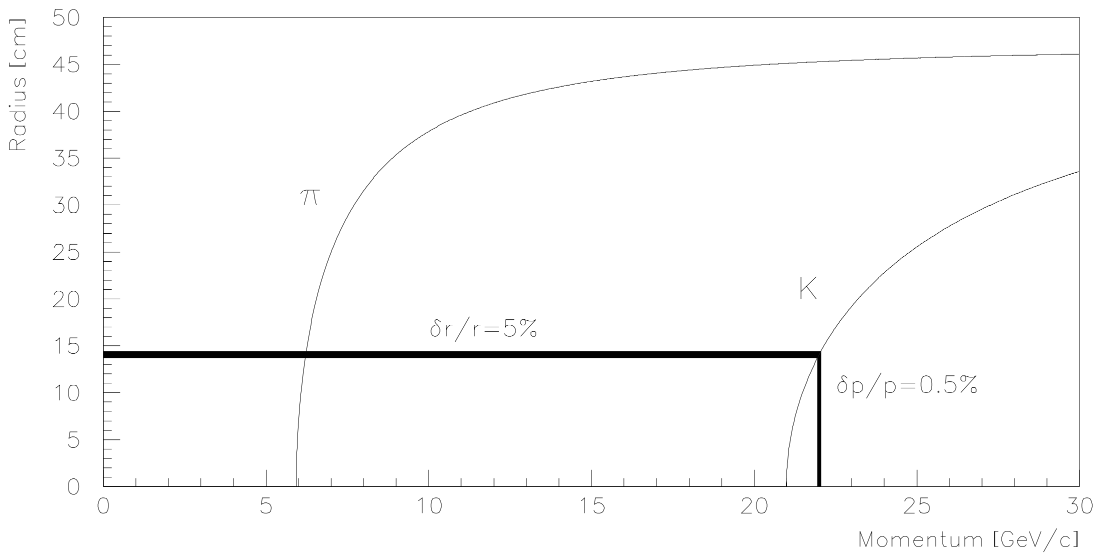

FIGURE 23. Expected ring radii for beam K^+ and pi^+ in the CKM KRICH.

resolution question is not appropriate to ask. The real question is: how Gaussian is the response function?

The design of the detectors is based on the SELEX RICH. In fig. 24 we show the result of a study with SELEX data, single track events with $\beta = 1$. To assign hits to a ring, we used the standard SELEX algorithm, which uses the information of the tracking system to determine the ring center. The average number of hits on a ring is 13.4, with a Poisson distribution. We fit a sum of Gaussian to this distribution, where the width of the Gaussian is scaled by $\sqrt{N-3}$ (N being the number of hits on a ring), and the weight is given by how many events we observed for every given N. As can be seen, the resolution function shows a Gaussian behavior over more than 4 orders of magnitude.

For CKM we do not want to use information from the tracking system in order to keep the two spectrometer systems really independent and redundant. We used the same SELEX sample as above, but this time performing a ring fit assigning *all* observed hits to the ring. We calculated the pull (deviation from mean divided by error) for the radius, where we scaled again the error with $\sqrt{N-3}$. The result is shown in fig. 25. The Gaussian behavior found in this study is already sufficient for the experiment. We are currently working on improving the pattern recognition algorithm. In addition, the

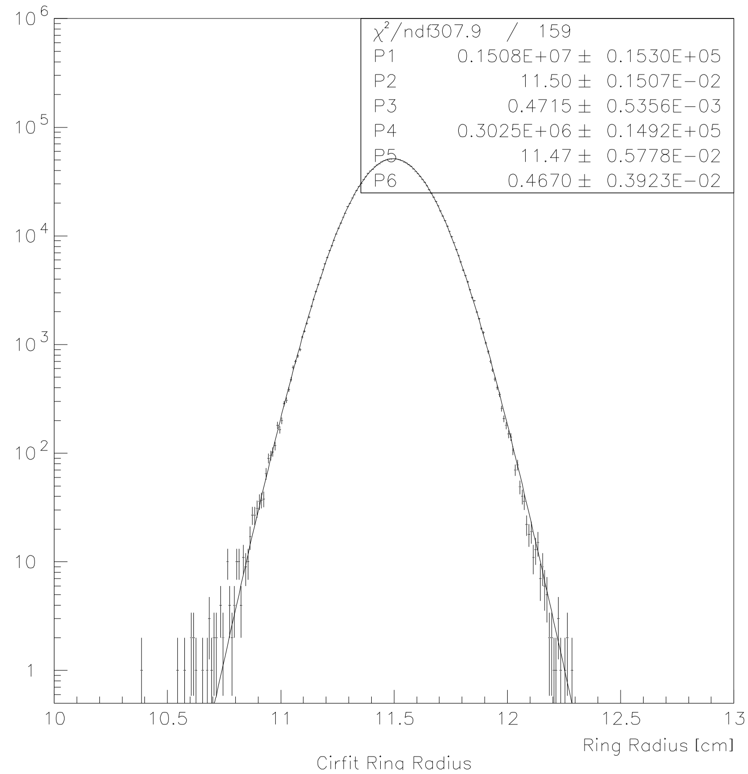

FIGURE 24. Ring radius distribution for $\beta = 1$ particles in the SELEX RICH, using the standard SELEX algorithm [44].

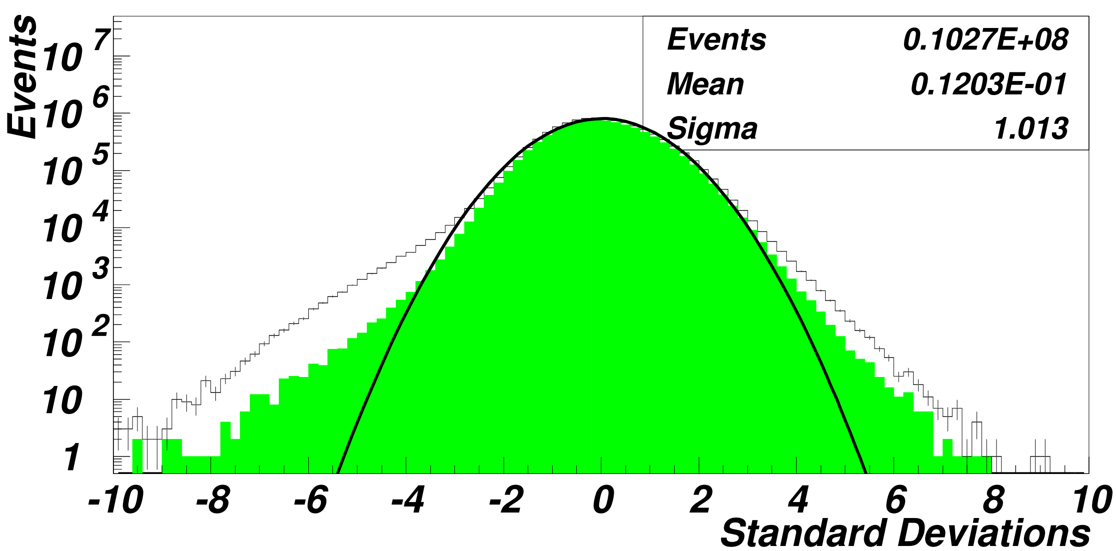

FIGURE 25. Pull distribution for the ring radius for $\beta = 1$ particles in the SELEX RICH. A simple standalone pattern recognition is used. The two histograms show no and a soft cut [44].

integration in SELEX was 170 nsec, and in CKM we expect a time resolution in the order of a few nsec, which should help to reduce the noise contribution.

TESTING CHERENKOV MIRRORS

The HEP group in San Luis Potosí, Mexico is involved in the design, construction, and testing of parts of for the CKM RICH detectors. We will mention here especially the construction and testing of mirrors. We apply the Ronchi method [39], which is shown

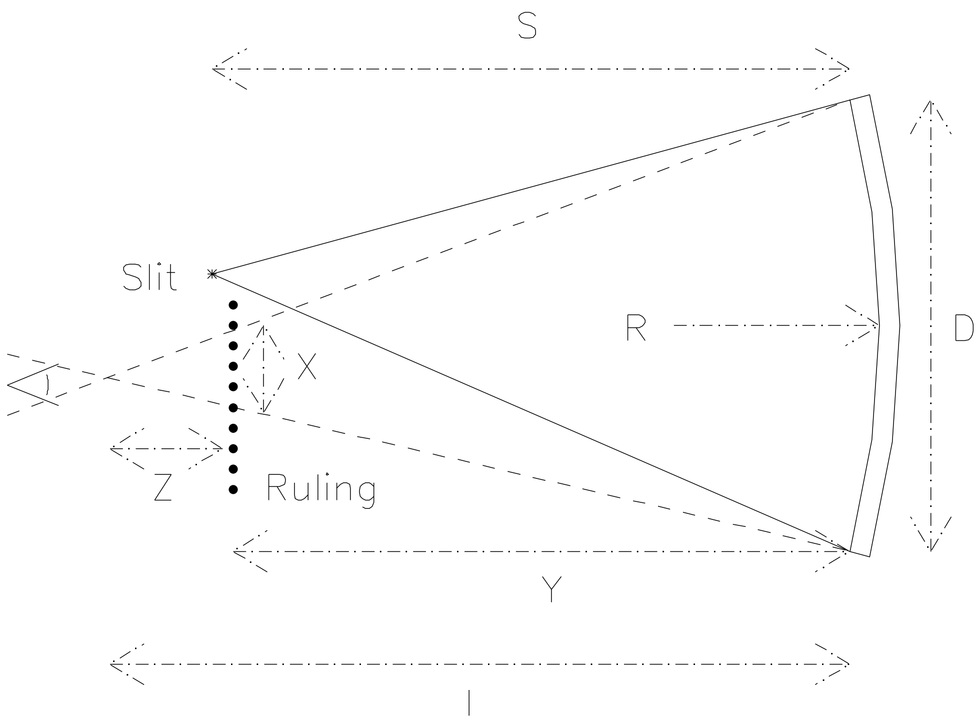

FIGURE 26. Principle idea of the Ronchi Method to measure the quality of spherical mirrors.

in fig. 26. The radius of a mirror is easily calculated, from the distance of the (nearly) parallel line. One obtains the following relations:

$$I = \frac{D \cdot Y}{D \mp G \cdot N_{\text{bands}}} \qquad\qquad \frac{1}{S} + \frac{1}{I} = \frac{2}{R}$$

With this method we are currently testing the first prototype mirrors produced in Mexico[3].

[3] CIO, León, Gto.

SUMMARY

We showed in this course that to identify charged particles one usually measures the velocity of the particle, identification is combined with the already known momentum.

Transition Radiation Detectors are mostly used in beam lines, but also to measure decay products (mostly electron–pion separation).

The Cherenkov effect is used in Threshold Cherenkov counters, and, since about 10 years, also in RICH detectors. RICHes are today an established standard detector technology, and several new experiments are planning to use RICH detectors as important components of their setup.

ACKNOWLEDGMENT

The author thanks the organizers of this school for the invitation and the possibility to give a course on his favored topic.

REFERENCES

1. C. Grupen: *Particle Detectors.* Cambridge University Press (1998).
2. R.C. Fernow: *Introduction to experimental particle physics.* Cambridge University Press (1986).
3. K. Kleinknecht: *Detectors for particle radiation.* Cambridge University Press, 2. english edition (1998).
4. J. Engelfried: *Experimental Techniques.* Proceedings of the VII Mexican Workshop on Particles and Fields, Merida, Mexico, November 10-17, 1999, 102-121, Preprint UASLP–IF–99–01, hep–ex/9912036.
5. SELEX Collaboration, F. Garcia et al.: *Hadronic Production of Λ_c from $600\,GeV/c$ π^-, Σ^- and p beams.* Physics Letters **B528** (2002), 49-57. Preprint Fermilab-Pub-01/258-E, hep-ex/0109017.
6. J. Russ et al., A proposal to construct SELEX, *Fermilab P781* (1987), unpublished.
   J. Russ, *Nucl. Phys.* **A585** (1995) 99.
   SELEX Collaboration, J.S. Russ *et al.*, in *Proceedings of the 29th International Conference on High Energy Physics*, 1998, edited by A. Astbury *et al.* (World Scientific, Singapore, 1998), Vol. II, p. 1259; hep-ex/9812031.
7. N. Terentyev et al.: *E781 Beam Transition Radiation Detector.* SELEX internal Note H-746.
8. B. Dolgoshein: *Complementary particle ID: transition radiation and dE/dx relativistic rise.* Nucl. Instr. and Meth. **A433** (1999) 533.
9. W. Brückner et al.: *The Transition Radiation Detector in the Hyperon Beam Experiment WA89 at CERN.* Nucl. Instr. and Meth. **A378** (1996) 451.
10. D. Errede et al.: *Use of a Transition Radiation Detector in a Beam of High-Energy Hadrons.* Nucl. Instr. and Meth. **A309** (1991) 386.
11. D. Errede et al.: *Design and Performance Characteristics of the E769 Beamline Transition Radiation Detector.* IEEE Trans. Nucl. Sci. **36** (1989) 106.
12. S. Paul: *Particle Identification using Transition Radiation Detectors.* CERN-PPE-91-199.
13. A. Roberts: *A new type of Cherenkov detector for the accurate measurement of particle velocity and direction.* Nucl. Instr. and Meth. **9** (1960) 55.
14. J. Séguinot and T. Ypsilantis: *Photo-ionization and Cherenkov Ring Imaging.* Nucl. Instr. and Meth. **142** (1977) 377.
15. E. Nappi, T. Ypsilantis (Eds.): *Proceedings of the First Workshop on Ring Imaging Cherenkov Detectors.* Nucl. Instr. and Meth. **A343** (1994) no. 1.

16. T. Ekelöf (Ed.): *Proceedings of the Second International Workshop on Ring Imaging Cherenkov Detectors.* Nucl. Instr. and Meth. **A371** (1996) no. 1/2.
17. A. Breskin, R. Chechik, T. Ypsilantis (Eds.): *Proceedings of the Third International Workshop on Ring Imaging Cherenkov Detectors.* Nucl. Instr. and Meth. **A433** (1999) no. 1/2.
18. *Proceedings of the IV. International Workshop on Ring Imaging Cherenkov Detectors.* Nuclear Instruments and Methods A, (2003).
19. P.A. Cherenkov: *Visible radiation produced by electrons moving in a medium with velocities exceeding that of light.* Phys. Rev. **52** (1937) 378.
20. I. Frank, I. Tamm: *Coherent visible radiation of fast electrons passing through matter.* C. R. Acad. Sci. URSS **14** (1937) 109.
21. A. Bideau-Méhu et al.: *Measurement of refractive indices of neon, argon, krypton, and xenon in the* $253.7-140.4$*nm wavelength range.* J. Quant. Spectrosc. Radiat. Transfer **25** (1981) 395.
22. H.-W. Siebert et al.: *The Omega-RICH.* Nucl. Instr. and Meth. **A343** (1994) 60.
23. J. Engelfried et al., A high-statistics experiment on the U(3100) and on charmed-strange baryons. *Letter of Intent CERN/SPSC/87-8, SPSC/I165* (1987).
24. A. Forino et al., Proposal for a new hyperon beam experiment at the CERN SPS using the Omega facility. *CERN/SPSC/87-43, SPSC/P233* (1987).
25. J. Engelfried: Ph.D. Thesis, Heidelberg University (1992), unpublished.
26. W. Beusch et al.: *The RICH counter in the CERN hyperon beam experiment.* Nucl. Instr. and Meth. **A323** (1992) 373.
27. U. Müller et al.: *The recent performance of the Omega RICH detector in experiment WA89 at CERN.* Nucl. Instr. and Meth. **A371** (1996) 27.
28. U. Müller et al.: *The Omega RICH in the CERN hyperon beam experiment.* Nucl. Instr. and Meth. **A433** (1999) 71.
29. R.A. Holroyd et al.: *Measurement of the absorption length and absolute quantum efficiency of TMAE and TEA from threshold to* 120 *nm.* Nucl. Instr. and Meth. **A261** (1987) 440.
30. J. Russ et al.: *A proposal to construct SELEX.* Fermilab P781 (1987), unpublished.
J. Russ: *Fermilab Hyperon Program: Present and Future Plans.* Nucl. Phys. **A585** (1995) 39c.
31. M.P. Maia et al.: *A Phototube RICH Detector.* Nucl. Instr. and Meth. **A326** (1993) 496.
32. V.A. Dorofeev et al.: *The Search for heavy Pentaquark Exotic Baryons with hidden Strangeness in the* $p+n \to (p\Phi)+n$ *and* $p+n \to (\Lambda(1520)K^+)+n$ *Reactions at* $E(p) = 70\,GeV$*.* Physics of Atomic Nuclei **57** (1994) 227.
33. A. Kozhevnikov et al.: *SPHINX Phototube RICH Detector for Diffractive Production Experiments at Serpukhov Accelerator.* Nucl. Instr. and Meth. **A433** (1999) 164.
34. J. Engelfried et al.: *The SELEX Phototube RICH Detector.* Nucl. Instr. and Meth. **A431** (1999) 53-69. hep-ex/9811001.
35. J. Engelfried et al.: *The E781 (SELEX) RICH Detector.* Nucl. Instr. and Meth. **A409** (1998) 439.
36. J. Engelfried et al.: *The RICH Detector of the SELEX Experiment.* Nucl. Instr. and Meth. **A433** (1999) 149.
37. J. Engelfried et al.: *SELEX RICH Performance and Physics Results.* Accepted for publication in Nuclear Instruments and Methods A. Preprint UASLP-IF-02-007, hep-ex-0208046
38. R. Richardson and R. Schmitt: Adv. in Cryo. Eng. **41B** (1996) 1907.
39. L. Stutte, J. Engelfried and J. Kilmer: *A Method to evaluate Mirrors for Cherenkov Counters.* Nucl. Instr. and Meth. **A369** (1996) 69.
40. U. Müller et al.: *Particle identification with the RICH detector in experiment WA89 at CERN.* Nucl. Instr. and Meth. **A343** (1994) 279.
41. I. Adam et al.: *Operation of the Cherenkov Detector DIRC of BABAR at High Luminosity.* SLAC–Pub–8783 (2001).
42. J. Schwiening: *The DIRC Detector at the SLAC B-Factory PEP-II: Operational Experience and Performance for Physics Application* Accepted for publication in Nuclear Instruments and Methods A. Preprint SLAC-PUB-7473.
43. R. Coleman et al.: CKM – Charged Kaons at the Main Injector – A proposal for a Precision Measurement of the Decay $K^+ \to \pi^+\nu\bar{\nu}$ and Other Rare K^+ Processes at Fermilab Using the Main Injector. FERMILAB-P-0905 (1998), unpublished.
CKM Collaboration, J. Frank et al., *CKM - Charged Kaons at the Main Injector - A proposal for a Precision Measurement of the Decay* $K^+ \to \pi^+\nu\bar{\nu}$ *and Other Rare* K^+ *Processes at Fermilab Using*

the Main Injector. Proposal (2nd edition) FERMILAB-P-0921, April 2001.

44. J. Engelfried et al.: *Two RICH Detectors as Velocity Spectrometers in the CKM Experiment*. Accepted by Nuclear Instruments and Methods A. Preprint UASLP-IF-02-008, Fermilab-Conf-02/192-E, hep-ex/0209020